IOP Publishing Measurement Science and Technology
Meas. Sci. Technol. 31 (2020) 055103 (13pp) https://doi.org/10.1088/1361-6501/ab62c5

A novel compound fault diagnosis method using intrinsic component filtering

Zongzhen Zhang, Shunming Li, Yu Xin and Huijie Ma

College of Energy and Power Engineering, Nanjing University of Aeronautics and Astronautics, Nanjing 210016, People's Republic of China

E-mail: zhzz18@126.com

Received 30 August 2019, revised 23 November 2019
Accepted for publication 17 December 2019
Published 26 February 2020

Abstract

The compound fault diagnosis of gearboxes, which can prevent breakdown accidents and minimize production loss, has become a challenging hotspot. In practical applications, the early fault signal is weak and often concealed by environmental noise. Therefore, separating the different fault components from signals with weak faults and strong noise is the key to performing compound fault diagnosis. In this paper, a novel compound fault diagnosis method based on intrinsic component filtering is proposed for compound fault diagnosis, which can also be regarded as a multi-dimension blind deconvolution method. Firstly, a Hankel matrix is constructed from the collected vibration data. Secondly, the filter matrix is trained by intrinsic component filtering in an unsupervised way without any time-consuming preprocessing or a prior basis. Finally, Hilbert demodulation analysis is conducted on the filtered data. Different fault components can be diagnosed according to the envelope spectra of the fault components. The separation performance of the proposed method is validated by the simulation data and the experiment signals in a noisy environment. The results show that the proposed method can train the different filters using the compound fault adaptively, demonstrating superior performance to existing methods.

Keywords: intrinsic component filtering, compound fault diagnosis, blind deconvolution, weak signature detection, gearbox

(Some figures may appear in colour only in the online journal)

1. Introduction

As an important transmission component in mechanical equipment, gearboxes are vital to the safety and reliability of mechanical equipment [1, 2]. In practical operation, when the gearbox has local faults, weak fault characteristic signals are always submerged in strong noise. Therefore, the compound fault diagnosis of gearboxes in noisy environments is of great importance in preventing breakdown accidents and minimizing production loss. In addition, due to the fact that the fault data collection time is obviously shorter than the analysis time, the rapid separation of different fault components from massive and complex data samples and the accurate identification of health conditions has become an urgent research subject [3, 4].

Due to its complex structure and poor working conditions, when a gear or bearing fails, it can easily induce other faults [5]. Compound fault diagnosis is much more difficult than single fault diagnosis, which is always a challenge for emerging techniques. Unlike single fault diagnosis, faults of a compound nature may interfere with each other. For example, there are different resonance bands in the frequency domain, and different impulse components in the time domain counteract or overlap with each other. In addition, the generation process of a compound fault is often a development process from a single fault to a compound fault. Therefore, the signal of a later fault in a compound fault is often weaker. In particular, for compound faults from bearings and gears, early gear faults may only produce an amplitude modulation phenomenon [6].

In early gear fault signals, the mesh frequency and its harmonics are modulated by the rotating speed [7]. By contrast, in a bearing fault signal, the inherent frequency of different fault conditions will be modulated by its characteristic

frequency [8]. In compound faults, the local faults of the gear and the bearing may co-exist and influence each other. Different fault component separation is at the core of compound fault diagnosis. In recent years, various data processing techniques have been proposed for compound fault separation such as empirical mode decomposition (EMD) [9–11], variational mode decomposition (VMD) [12, 13], the envelope analysis method, maximum correlated kurtosis deconvolution (MCKD) [14–16], morphological compound analysis (MCA) [17] and the kurtogram [18, 19], etc. Antoni elaborated on the related theories of SK and officially gave a mathematical definition of it, which was the energy-normalized fourth-order spectral cumulant. Then, a fast kurtogram concept was proposed, which has been studied and is being widely used by more and more researchers [20–22]. Wavelet packet transform (WPT) filters can process nonstationary transient vibration signals more efficiently than STFT. Therefore, Lei *et al* proposed an improved kurtogram in which STFT is replaced with WPT [23]. To solve the problem of the kurtogram tending to choose the frequency band with individual impulses rather than the desired fault impulses, Miao *et al* introduced a sparsity index called the Gini index as an alternative estimator for the selection of the resonance band [24]. The improvement method is more effective under harsh working conditions, even in complex structures. These methods have played important roles in the fault diagnosis of gearboxes.

However, the approaches may suffer some kinds of limitation. EMD, VMD, and envelope analysis are effective tools for extracting harmonic features but not valid for the detection of transient features. In addition, the performance of these methods will be degraded with a low signal-to-noise ratio (SNR). Therefore, these kinds of method usually need to be carried out with noise reduction technology. Morphological component analysis (MCA) approaches this problem via sparse representation and dictionary learning [25]. The main idea behind MCA is to use the morphological diversity of the different faults contained in the data to associate each morphology to a dictionary of atoms for which a fast transform is available [25]. In [26], Db, Symmlet and Coiflet wavelets are selected to represent the periodic impulse component, and local discrete cosine and sine dictionaries (LDCS) are selected to represent the meshing component. However, MCA cannot separate multiple bearing faults due to the fact that the dictionary we choose will extract different impulse components as one fault. MCKD is an effective tool for separating out the periodic impulse fault component from the vibration signal in the case of strong background noise [14]. In [27], MCKD is used to separate the different fault components from the compound bearing fault signal. However, the main problem in the practical application of MCKD is how to set the following four parameters appropriately: the length of the filter, the maximum count of iteration, and the order of the shift and fault period, which will affect the performance of the MCKD [14]. It should be noticed that MCA and MCKD require an *a priori* basis and the selection of proper parameters is difficult, limiting their use in practical applications.

Sparse filtering, which was first proposed by Ngiam [28], is a simple and effective method and has been widely used in the area of intelligent fault diagnosis [29, 30]. In [31], Jia developed the application of sparse filtering and proposed a convolutional sparse filter (CSF) for weak signature detection. One-dimensional CSF shows the advantages of strong noise adaptability, a fast filter training process and the need for few parameters to be adjusted [32]. However, the filter training performance and robustness of the CSF will be degraded in the case of multi-dimensions especially for harmonic components. Meanwhile, it needs a large output dimension to train the filters more accurately.

To overcome these weaknesses, a novel compound fault diagnosis method based on intrinsic component filtering is proposed to separate the compound fault in an unsupervised way. The simulation and experimental results show that the proposed method can effectively separate the gear fault component and the bearing fault component from the compound fault vibration signals of gearboxes with stronger noise adaptability.

The main contributions of this literature are summarized as follows. Firstly, the filter learning process of the proposed method is unsupervised and has only two simple tunable hyperparameters: input dimension and output dimension. Secondly, the proposed method does not require any prior knowledge in the process of fault separation. Thirdly, the proposed method is applicable to various fault compound modes, and is an effective tool for both harmonic and transient features.

The rest of this paper is organized as follows. The application of CSF in weak signature detection is introduced in section 2. In section 3, the proposed method is described in detail. The simulated and experimental results are analyzed and discussed in section 4. Finally, conclusions are drawn in section 5.

2. Convolutional sparse filtering

Sparse filtering, which was first proposed by Ngiam [18], is a simple and effective method which has three desired principles: population sparsity, lifetime sparsity and high dispersal through the optimization of the $l_{1/2}$ norm of the normalized feature matrix. In recent research, sparse filtering methods are used to extract discriminative features adaptively from original vibration signals in an unsupervised way. Then, the features are fed to a classifier, such as softmax regression, to classify the health conditions in a supervised manner [29, 30].

Sparse filtering is viewed as a two-layer neural network. The objective function of sparse filtering can be written as

$$J_{\mathrm{SF}}(\boldsymbol{f}) = \sum_{1}^{m} \left\| \frac{\hat{\boldsymbol{f}}^{i}}{\left\| \hat{\boldsymbol{f}}^{i} \right\|_2} \right\|_1 \quad \text{where} \hat{\boldsymbol{f}}_j = \frac{\boldsymbol{f}_j}{\left\| \boldsymbol{f}_j \right\|_2} \tag{1}$$

where $\boldsymbol{f}_j^i \in \Re^{N_{\mathrm{out}} \times M}$ corresponds to the jth feature of the ith sample, which is computed using a weight matrix and the training samples $\left\{\boldsymbol{x}^i\right\}_{i=1}^{M}$, and $\boldsymbol{x}^j \in \Re^N$ is the original signal.

A sparse feature learning method can also be used as a blind deconvolution method for weak signature detection. Jia developed the application of sparse filtering of the vibration signal processing to pursue finer solutions for weak

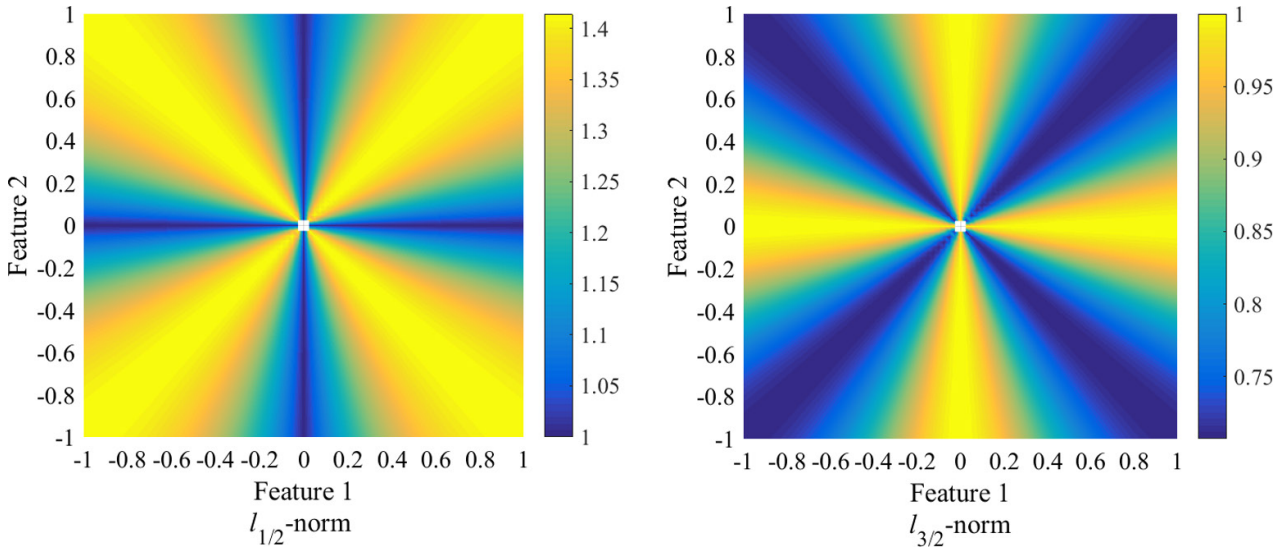

Figure 1. The $l_{1/2}$-norm and the $l_{3/2}$-norm of a 2D vector.

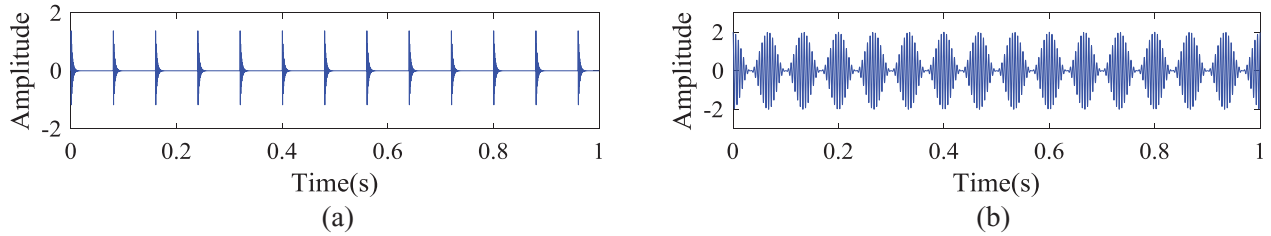

Figure 2. The time domain waveform of the simulated vibration signal: (a) the bearing fault, (b) the gear fault.

impulsive signature enhancement. The derivation of the CSF is presented in detail in [21]. The input matrix of the CSF is a Hankel matrix constructed by the input data $\boldsymbol{x}^j \in \Re^N$, which can be expressed as

$$\boldsymbol{H} = \begin{bmatrix} x_1 & x_2 & x_3 & \cdots & x_{N-L+1} \\ x_2 & x_3 & x_4 & \cdots & x_{N-L+2} \\ x_3 & x_4 & x_5 & \cdots & x_{N-L+3} \\ \vdots & \vdots & \vdots & \vdots & \vdots \\ x_L & x_{L+1} & x_{L+2} & \cdots & x_N \end{bmatrix}. \tag{2}$$

Multiple inverse filters will be obtained from the CSF using the weight matrix. In the output layer, only the dominant features of the feature matrix are preserved by using dimension reduction technology. One-dimensional sparse filtering shows good performance in weak signal detection. The weight vectors calculated by multi-dimensional sparse filtering need PCA dimensionality reduction, which improves the noise reduction effect of the CSF. However, in compound fault diagnosis, the robustness of the feature learning performance of the filter is poor, especially for the harmonic component.

3. The proposed method

3.1. Intrinsic component filtering

Recent literature [30] has developed the normalization method of sparse filtering as a generalized $l_{r-p/q}$ form, as shown in equation (3). A sparse distribution can be achieved by minimizing $J_{\text{gnsp}}(x)$ for the case of $p < q$, or maximizing $J_{\text{gnsp}}(x)$ when $p > q$. The research results show better performance in case of $p = 3, q = 2, r = 2$:

Table 1. The parameters of the simulated signals.

Number	f_s	f_r	T_b	α	A
S_1	20 kHz	2000 Hz	0.025 s	300	1
S_2	20 kHz	1200 Hz	0.04 s	500	0.7

$$J_{\text{gnsf}}(\boldsymbol{f}) = \left(\frac{1}{N}\right)^{1-\frac{p}{q}} \cdot \sum_i^M \frac{\left(\sum_j^N \left|\hat{\boldsymbol{f}}^i\right|^p\right)}{\left(\sum_j^N \left|\hat{\boldsymbol{f}}^i\right|^q\right)^{\frac{p}{q}}} \tag{3}$$

where $\hat{\boldsymbol{f}} = f_j / \left(\sum_j^N \left|\boldsymbol{f}_j\right|^r\right)^{\frac{1}{r}}$ and $p \neq q$.

Intrinsic component filtering focuses on the consistency between the samples with the same condition. The $l_{1/2}$-norm of the column of the feature matrix is used to realize the sparsity of features per sample and the $l_{3/2}$-norm of the rows is used to achieve consistency of features between the samples.

Specifically, the training samples of the Hankel matrix are mapped onto their features $\boldsymbol{f}_j^i \in \Re^{N_f \times (N-L+1)}$ using a weight matrix $\boldsymbol{W} \in \Re^{N_f \times L}$, where the $\boldsymbol{x}^i \in \Re^{N \times 1}$ is a training sample, N_f is the filter number, and L denotes the filter length and the input dimension of ICF:

$$\boldsymbol{f} = \boldsymbol{W}\boldsymbol{x}. \tag{4}$$

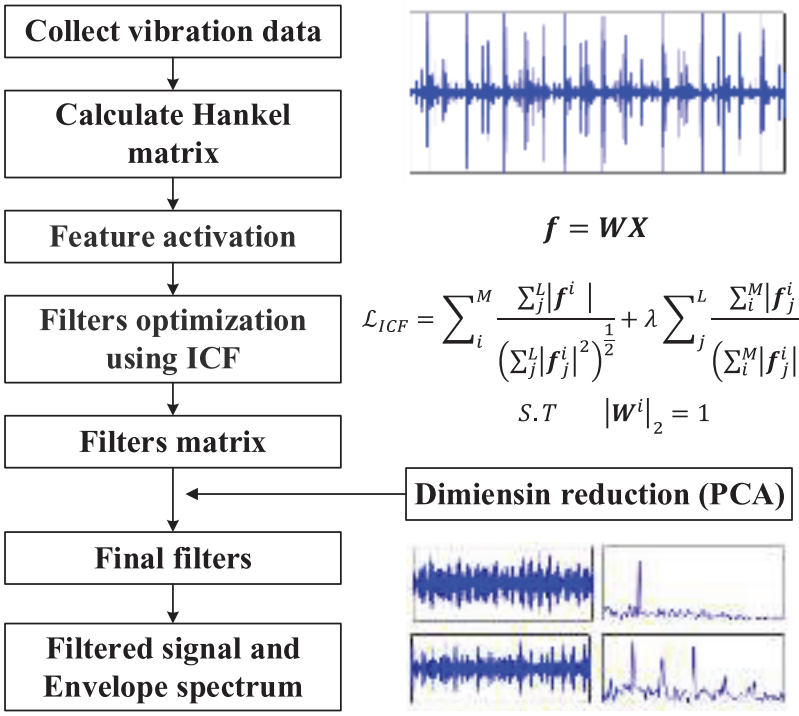

Figure 3. A flow chart of the proposed method.

The $l_{1/2}$-norm is employed to achieve the sparsity of features per sample. The $l_{3/2}$-norm of rows is used to achieve the consistency of features between the samples. In order to eliminate the influence of redundancy in the optimization process, the weight vectors are constrained to the unit vectors. The final objective function of the ICF can be written as

$$\mathcal{L}_{\mathrm{ICF}} = \sum_i^M \frac{\sum_j^{N_f} \left|f_j^i\right|}{\left(\sum_j^{N_f} \left|f_j^i\right|^2\right)^{\frac{1}{2}}} + \lambda \sum_j^{N_f} \frac{\sum_i^M \left|f_j^i\right|^3}{\left(\sum_i^M \left|f_j^i\right|^2\right)^{\frac{3}{2}}} \quad S.T \ |W^i|_2 = 1 \tag{5}$$

where $M = N - L + 1$, $\mathcal{L}_{\mathrm{ICF}}$ is nonsmooth and nonconvex, and we replace $|f|$ with the soft-absolute function $\sqrt{f^2 + \varepsilon}$, where ε is a small positive number and has the value 1×10^{-8} in this paper. Then, we take the off-the-shelf algorithm L-BFGS to minimize the objective function until convergence. The gradient function is given by

$$\frac{\partial \mathcal{L}_{\mathrm{ICF}}}{\partial \boldsymbol{w}} = \left[\left(\frac{\boldsymbol{O}}{\left(\sum_j^{N_f} \left|f^i\right|^2\right)^{\frac{1}{2}}} - \frac{f \cdot \sum_j^{N_f} \left(f^i\right)}{\left(\sum_j^{N_f} \left|f^i\right|^2\right)^{\frac{3}{2}}} \right) + 3\lambda \left(\frac{\sum_i^M \left(f_j\right)^2}{\left(\sum_i^M \left|f_j\right|^2\right)^{\frac{3}{2}}} - \frac{f \cdot \sum_i^M \left(f_j^3\right)}{\left(\sum_i^M \left|f_j\right|^2\right)^{\frac{5}{2}}} \right) \right] \cdot g_{\mathrm{a}} \cdot \frac{f}{|f|} \cdot x' \tag{6}$$

where $\boldsymbol{o} \in \Re^{N_{\mathrm{out}} \times M}$ is a matrix of all ones and g_{a} is the gradient of the activation function.

The $l_{1/2}$-norm and $l_{3/2}$-norm of a 2D vector is plotted in figure 1 to further explain the characteristics of ICF. It can be seen that the minimum value of the $l_{1/2}$-norm is on the coordinate axis. In this case, one of the values of the two features is 0, which means that the ratio of the two features is much greater (or less) than 1. However, the maximum value of the $l_{1/2}$-norm is on the coordinate axis and the ratio of the two features equals 1. Similarly, the maximum value of the $l_{3/2}$-norm is on the coordinate axis and the minimum value is on the diagonal line. Therefore, the minimization of the $l_{1/2}$-norm means sparsity and the minimization of the $l_{3/2}$-norm means the features are equal.

3.2. Compound fault separation using ICF

In this paper, a novel multi-dimension blind deconvolution method is proposed based on the ICF algorithm for rotating machinery compound fault separation. The framework of the proposed method is shown in figure 3 and the main steps are described as follows.

Step 1: The construction of the training matrix using row data. Suppose that the input dimension and output dimension of the ICF are L and N_{f}. Specifically, the collected signal $x \in \Re^N$ is transformed into a Hankel matrix $\boldsymbol{H} \in \Re^{L \times (N-L-1)}$. Each ascending skew-diagonal element from left to right is constant in the Hankel matrix.

Step 2: Filter optimization using ICF. This is an unsupervised learning process and multiple inverse filters are obtained.

Step 3: Signal filtering through trained filters.

Step 4: Dimension reduction using PCA. The first order principal components are selected as the final signals.

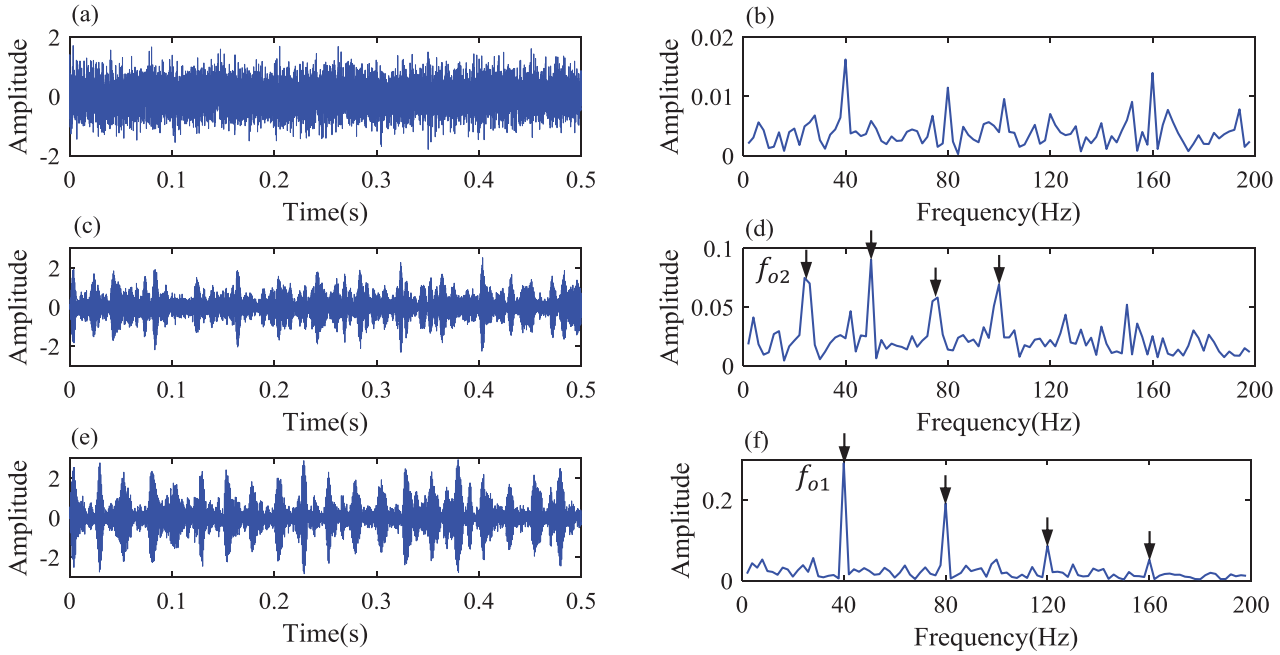

Figure 4. Diagnosis results of the bearing compound fault using ICF. (a) A simulated compound fault vibration time series with SNR $= -10$ dB; (b) the envelope spectrum of the simulated signal; (c) the time waveform of the filtered signal of S_2; (d) the envelope spectrum of the filtered data of S_2; (e) the time waveform of the filtered data of S_1; (f) the envelope spectrum of the filtered data of S_1.

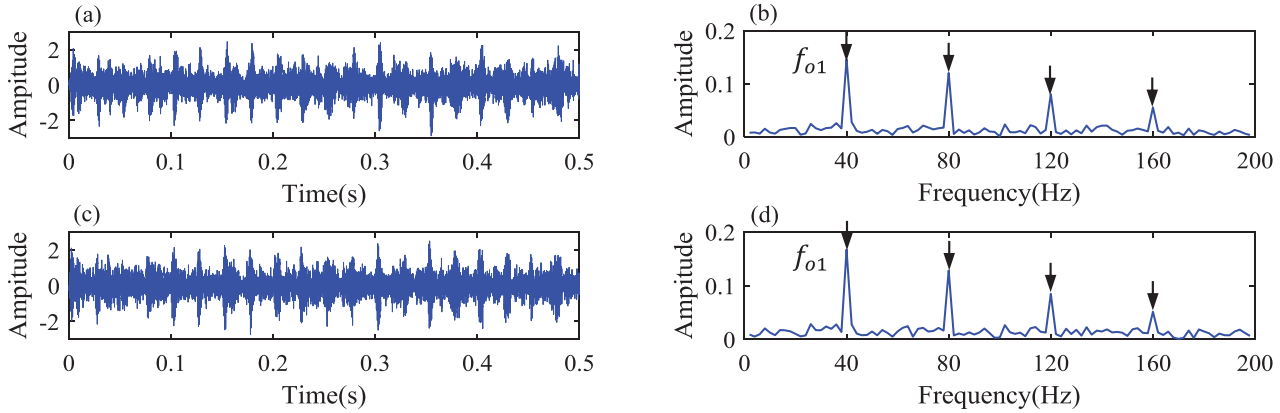

Figure 5. The diagnosis results of the bearing compound fault using CSF. (a) The time waveform of the filtered data of component 1; (b) the envelope spectrum of the filtered data of component 1; (c) the time waveform of the filtered data of component 2; (d) the envelope spectrum of the filtered data of component 2.

4. Simulation analysis

In this section, application of the ICF for compound fault diagnosis is demonstrated based on the simulated signals.

4.1. Case 1: compound fault of bearings

The simulated vibration signals of the bearing outer-race failure are shown in figure 2(a), which can be expressed as follows:

$$x(t) = \sum_i AB(t) S_{\mathrm{b}}(t - \mathrm{i}T_{\mathrm{b}} - \delta T) + n(t) \tag{7}$$

$$B(t) = [1 - \cos(2\pi f_{\mathrm{r}} t)]/2 \tag{8}$$

$$S_{\mathrm{b}}(t) = \mathrm{e}^{-\alpha t} \sin(2\pi f_{\mathrm{r}} t) \tag{9}$$

where A simulates the amplitude coefficient, and $B(t)$ is the amplitude modulation due to the effects of the transmission path. $S_{\mathrm{b}}(t)$ expressed as equation (9) is the impulse response function of the bearing-casing-sensor system which represents periodic impulse components when it is simplified as a linear system. T_{b} represents the time interval between two impulses, which means the frequency of the shock is $1/T_{\mathrm{b}}$. δT denotes the random jitter caused by the slip effect of rolling elements. f_{r} specifies the resonant frequency that is excited by mechanical defects and α is the decay rate of the impulses. $n(t)$ is the noise component to simulate random interference, which is simulated as Gaussian noise. The definition of the signature to noise ratio (SNR) is expressed as

$$\mathrm{SNR_{dB}} = 10\log_{10}\left(\frac{P_{\mathrm{signal}}}{P_{\mathrm{noise}}}\right) \tag{10}$$

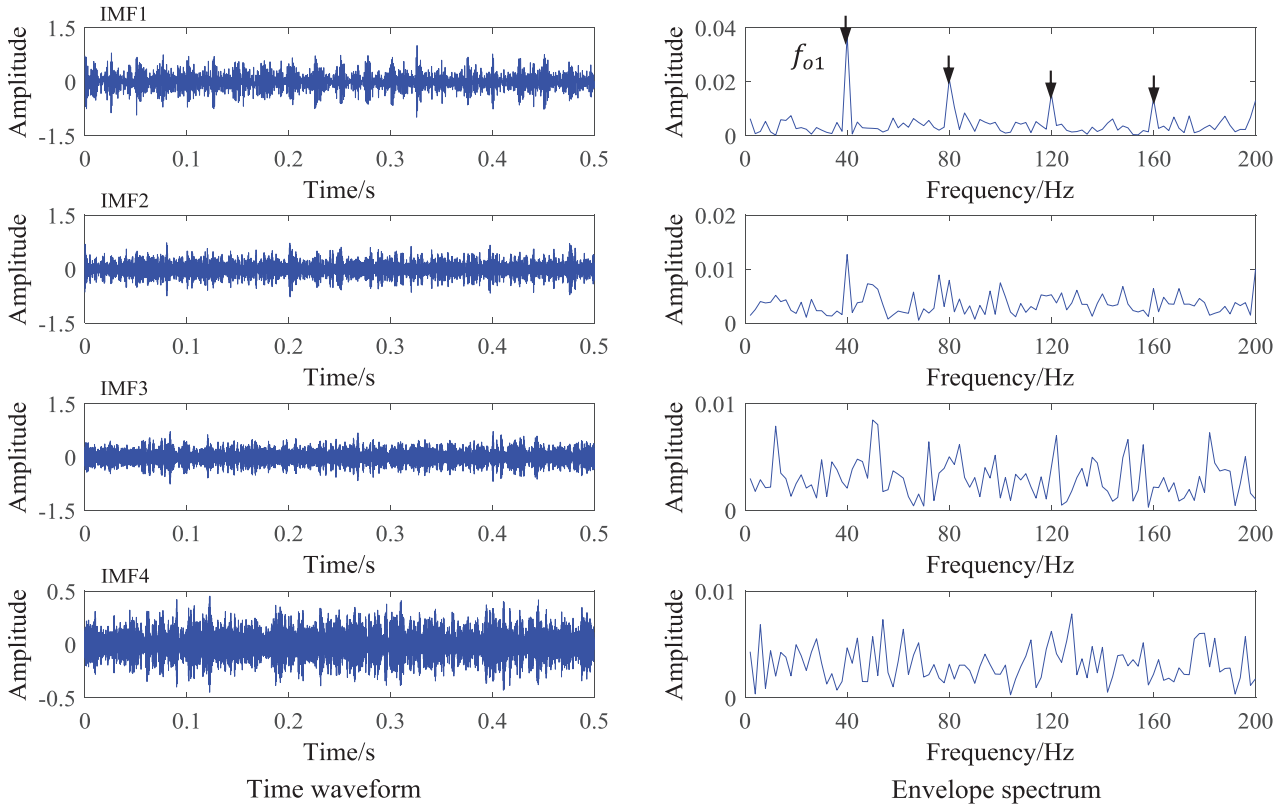

Figure 6. Decomposition results bearing the compound fault using VMD.

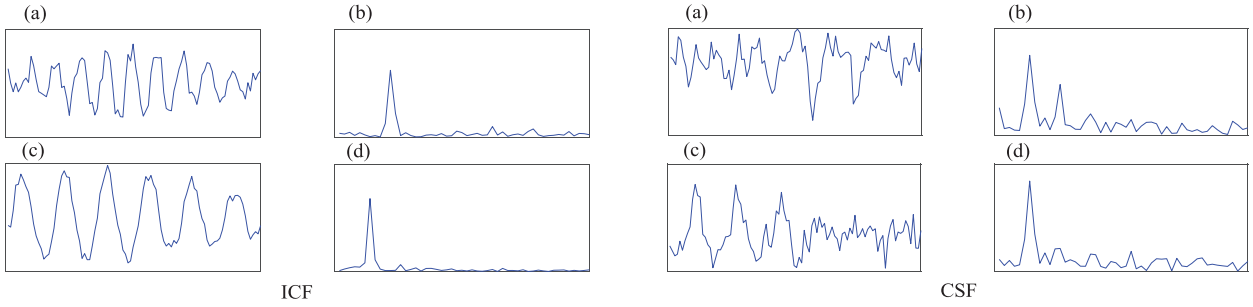

Figure 7. The filters of the bearing compound fault trained by ICF and CSF and the corresponding spectrum. (a) The time waveform of the trained filter of S_1; (b) the envelope spectrum of the trained filter of S_1; (c) the time waveform of the trained filter of S_2; (d) the envelope spectrum of the trained filter of S_2.

where P_{signal} and P_{noise} are the power of the signal and the noise respectively. The parameter settings of the simulated signals in this section are displayed in table 1.

In this experiment, the output dimension of the ICF is 10, $\lambda = 1$, $L = 100$. The detection results using ICF and CSF and the corresponding envelope spectra are plotted in figures 4 and 5 with SNR $= -10$ dB. The results indicate that the proposed ICF can separate different impulsive signatures with various amplitudes from the compound fault signal. Two filtered components extracted by the ICF can successfully detect the different bearing fault from the envelope spectrum. The peak values are obvious at the characteristic frequency (40 and 25 Hz) and its harmonics, which indicates that an outer ring fault has occurred. In addition, the ICF filters recover the impulsive signature of the input signal successfully in the time domain. However, CSF can only extract the feature of S_1 as shown in figure 4. It is difficult to identify the fault in S_2 through the filtered time domain signal and envelope spectrum, due to the vibration amplitude of S_2 being smaller. The decomposition results using VMD are displayed in figure 6. The balancing parameter of the data-fidelity constraint is set as 2000 and the number of modes to be recovered is four. It can be seen that the decomposition results of VMD are similar to those of CSF: they can only identify the fault characteristics of S_1. We can see the obvious shock information from the first IMF, and the corresponding envelope spectrum has obvious peaks in the characteristic frequency of S_1. The recovered time domain waveform of ICF is the best of the three methods.

In order to study the property of the proposed ICF, the trained filters corresponding to the different fault components and their spectrum are displayed in figure 7. It can be seen that the first two principal components correspond to two fault

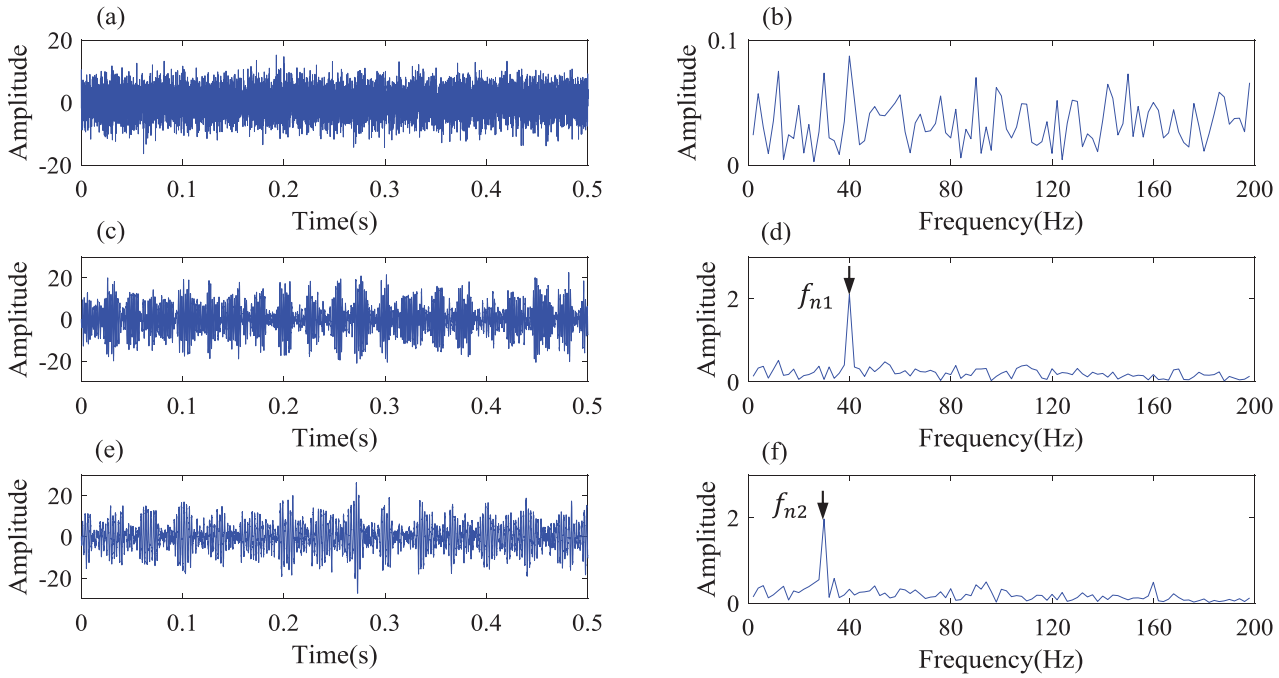

Figure 8. The diagnosis results of compound gear faults using ICF. (a) A simulated compound fault vibration time series with SNR $= -10$ dB; (b) the envelope spectrum of the simulated signal; (c) the time waveform of the filtered data of S_3; (d) the envelope spectrum of the filtered data of S_3; (e) the time waveform of the filtered data of S_4; (f) the envelope spectrum of the filtered data of S_4.

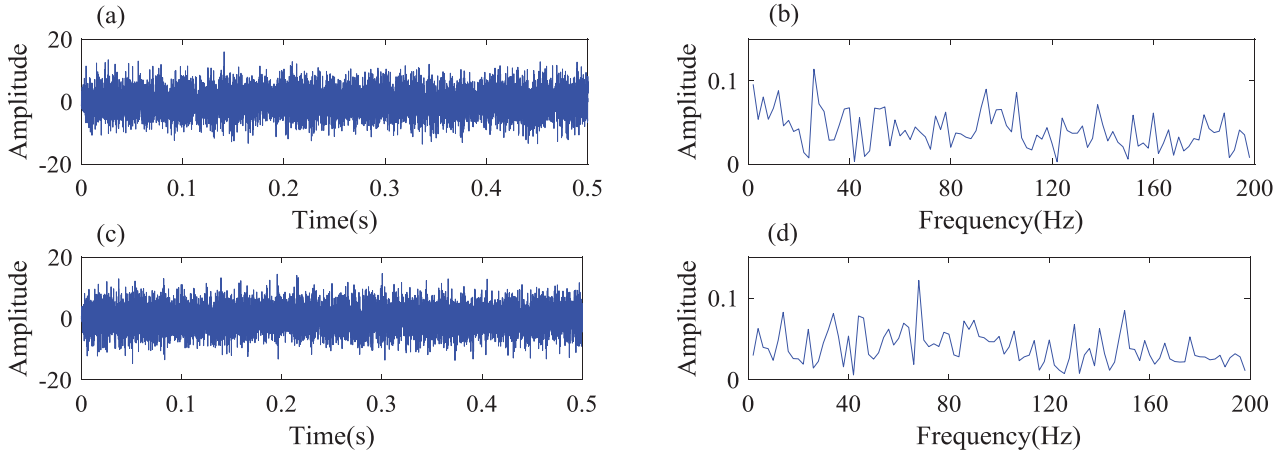

Figure 9. The diagnosis results of compound gear faults using CSF. (a) The time waveform of the filtered data of S_3; (b) the envelope spectrum of the filtered data of S_3; (c) the time waveform of the filtered data of S_4; (d) the envelope spectrum of the filtered data of S_4.

characteristics. The main frequencies of the filters trained by the ICF are the resonant frequency of S_1 and S_2, respectively. This further explains why ICF can accurately separate different fault components. The resonant frequency of S_2 is successfully trained by CSF, however, the filter corresponding to S_1 still contains the characteristics of S_2. Therefore, compared with CSF, ICF shows superior performance in the decomposition of compound bearing faults.

4.2. Case 2: compound fault of gears

The vibration signal of the gearbox fault contains amplitude and phase modulations that are periodic with the frequency of rotation of the gear, which can be simulated as

$$h(t) = \sum_{m=0}^{M} X_m(1 + a_m(t))\cos(2\pi m z f_n t + \phi_m + b_m(t)) + n(t) \tag{11}$$

where M simulates the number of tooth-meshing harmonics; f_n is the rotating frequency; z denotes the number teeth of the gear; and X_m and ϕ_m denote the amplitude and the phase of the mth meshing harmonic, respectively. a_m and b_m are the amplitude and phase modulation functions, respectively. The time domain waveform of the simulated gear fault vibration signal is shown in figure 3(b). In this experiment, the output dimension of ICF is 10, $\lambda = 1$, $L = 100$. The sampling frequency is set as 20kHz, the rotating frequency f_n is set as 30 Hz and 40Hz, and the number of teeth of the gear z are set as 13 and 14. The corresponding signal numbers are S_3 and S_4.

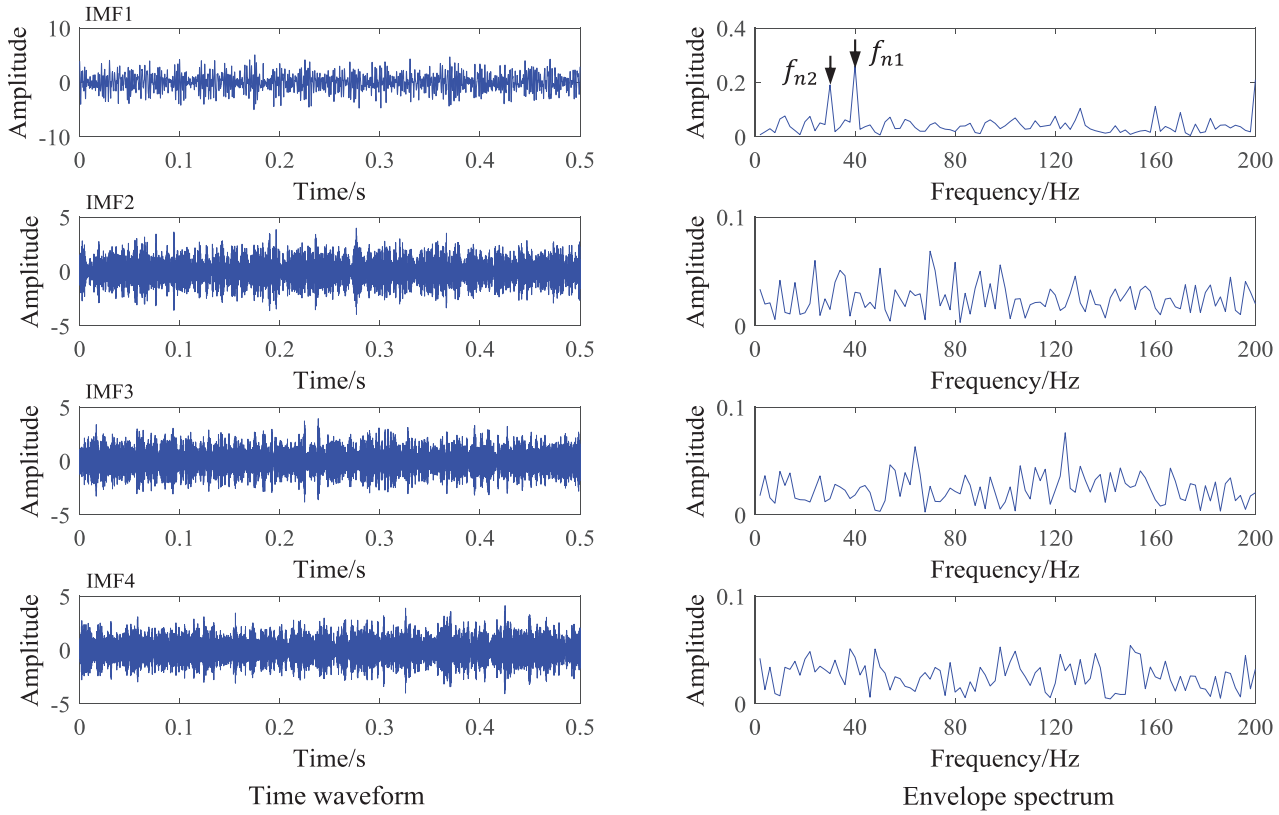

Figure 10. The decomposition results of the gear compound fault using VMD.

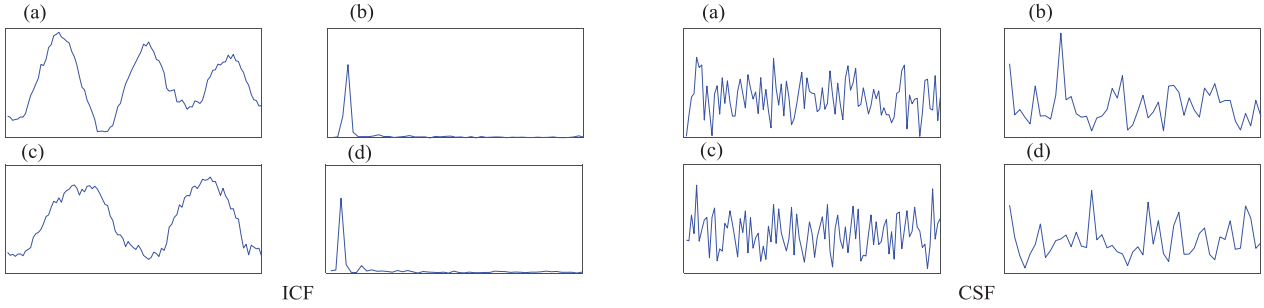

Figure 11. The filters of compound gear faults trained by ICF and CSF and the corresponding spectrum. (a) The time waveform of the trained filter of S_3; (b) the envelope spectrum of the trained filter of S_3; (c) the time waveform of the trained filter of S_4; (d) the envelope spectrum of the trained filter of S_4.

The experiment results using ICF and CSF and the corresponding envelope spectra are plotted in figures 8 and 9 with SNR $= -10$ dB. It can be seen that it is difficult to find the fault information in the original signal, due to the interaction of two faults and the influence of noise. The proposed ICF can separate different harmonic features from the compound fault signal in a noisy environment. The different gear faults are separated by the two filters (the first two principal components) of ICF and it can be successfully detected from the corresponding envelope spectrum. In figures 8(d) and (f), there is an obvious peak at the rotating frequency 30 and 40 Hz, which corresponds to the crack fault of the gear. In addition, the ICF filters recover the impulsive signature of the input signal successfully in the time domain, as shown in figures 8(c) and (e). By comparison, as shown in figure 9, no components have been observed in the first two principal features extracted by CSF. It is difficult to distinguish the fault in the gear. These results show that CSF cannot extract different gear fault features simultaneously due to the interference of noise.

The decomposition results using VMD are displayed in figure 10. It can be seen that the envelope spectrum of the first IMF contains two main frequencies, which means that two fault features are extracted simultaneously without achieving separation of the different fault components.

The trained filters corresponding to the different fault components and their spectra are displayed in figure 11. It can be seen that the main frequencies of the filters trained by ICF correspond to the gear meshing frequency of S_3 and S_4, respectively. However, there is no obvious frequency component for

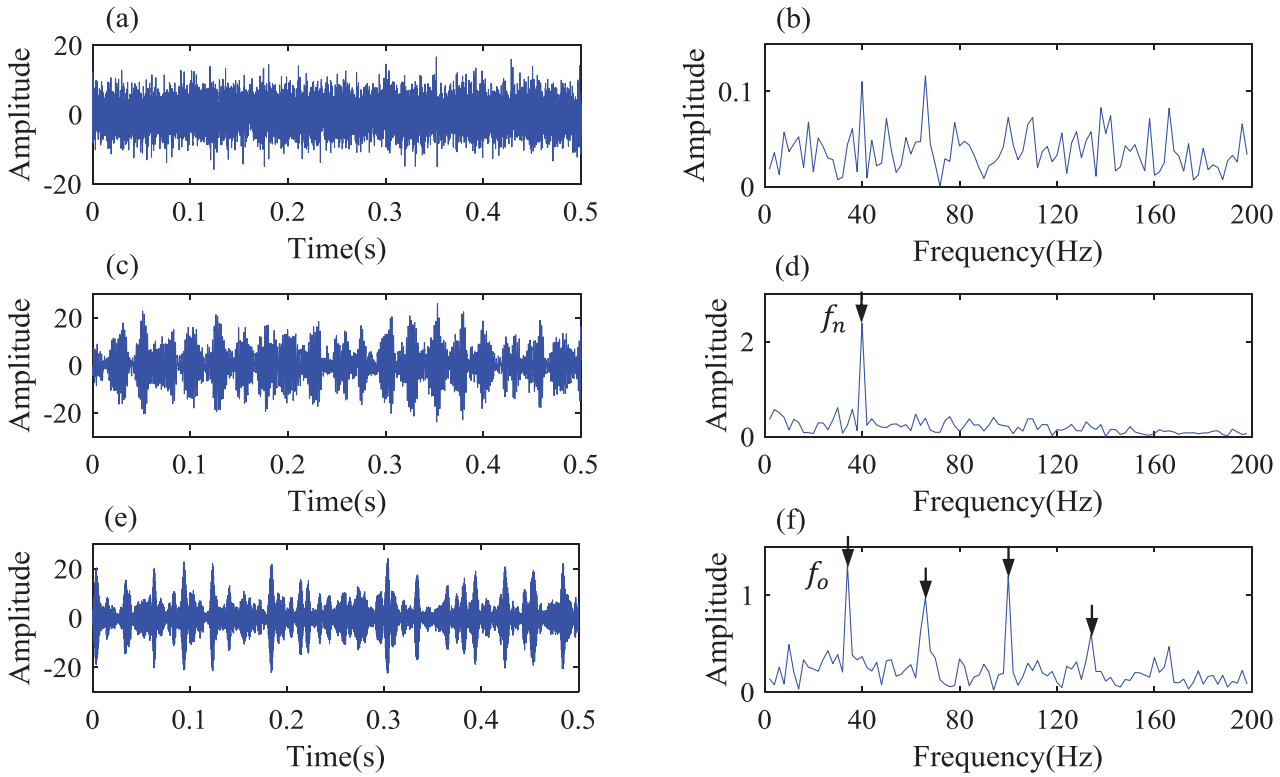

Figure 12. The diagnosis results of the gear and bearing compound fault using ICF. (a) A simulated compound fault vibration time series with SNR $= -10$ dB; (b) the envelope spectrum of the simulated signal; (c) the time waveform of the filtered data of the gear fault component; (d) the envelope spectrum of the filtered data of the gear fault component; (e) the time waveform of the filtered data of the bearing fault component; (f) the envelope spectrum of the filtered data of the bearing fault component.

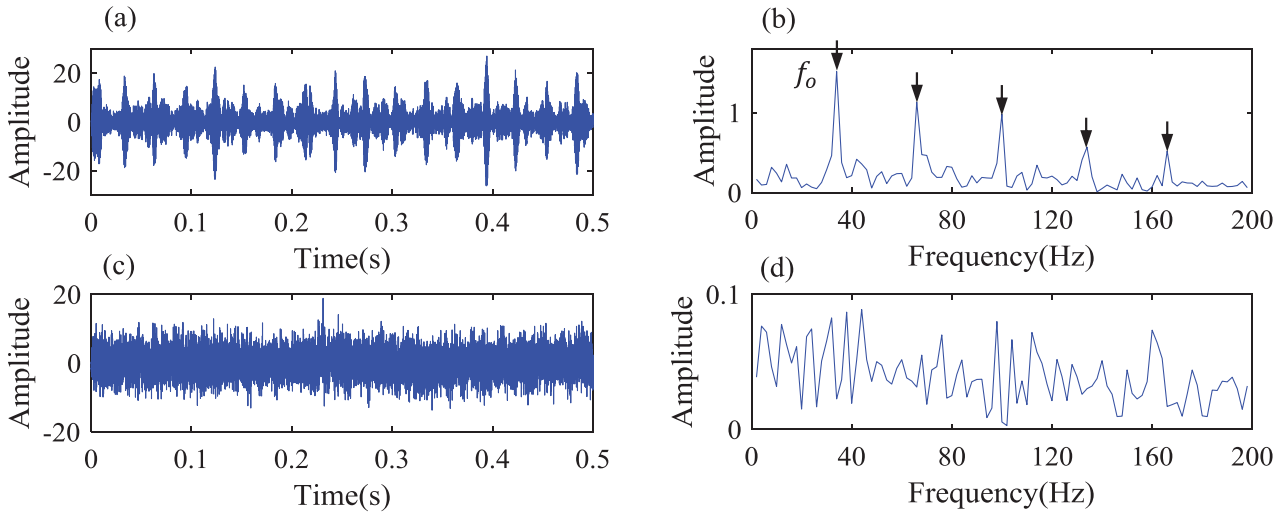

Figure 13. The diagnosis results of the gear and bearing compound fault using CSF. (a) The time waveform of the filtered data of the gear fault component; (b) the envelope spectrum of the filtered data of the gear fault component; (c) the time waveform of the filtered data of the bearing fault component; (d) the envelope spectrum of the filtered data of the bearing fault component.

the filters trained by CSF. This indicates that CSF will not over-sparsify the harmonic signal. Therefore, compared with CSF, ICF shows more superior performance in the separation of compound gear faults.

4.3. Case 3: compound fault of gear and bearing

In this experiment, the output dimension of ICF is 10, $\lambda = 1, L = 100$. The first two principles of the trained filters are selected as the final filters. The detected results using ICF, CSF and VMD are plotted in figures 12–14 with SNR $= -10$ dB. Figures 12(a) and (b) show the raw compound fault signal and its envelope spectrum. It is difficult to judge the fault information with them. The first two principles of the filters trained by ICF and the first two IMFs calculated by VMD can successfully separate the harmonic and transient component and recover the input signal in the time domain. ICF recovers the fault data better in the time domain. However, in comparison,

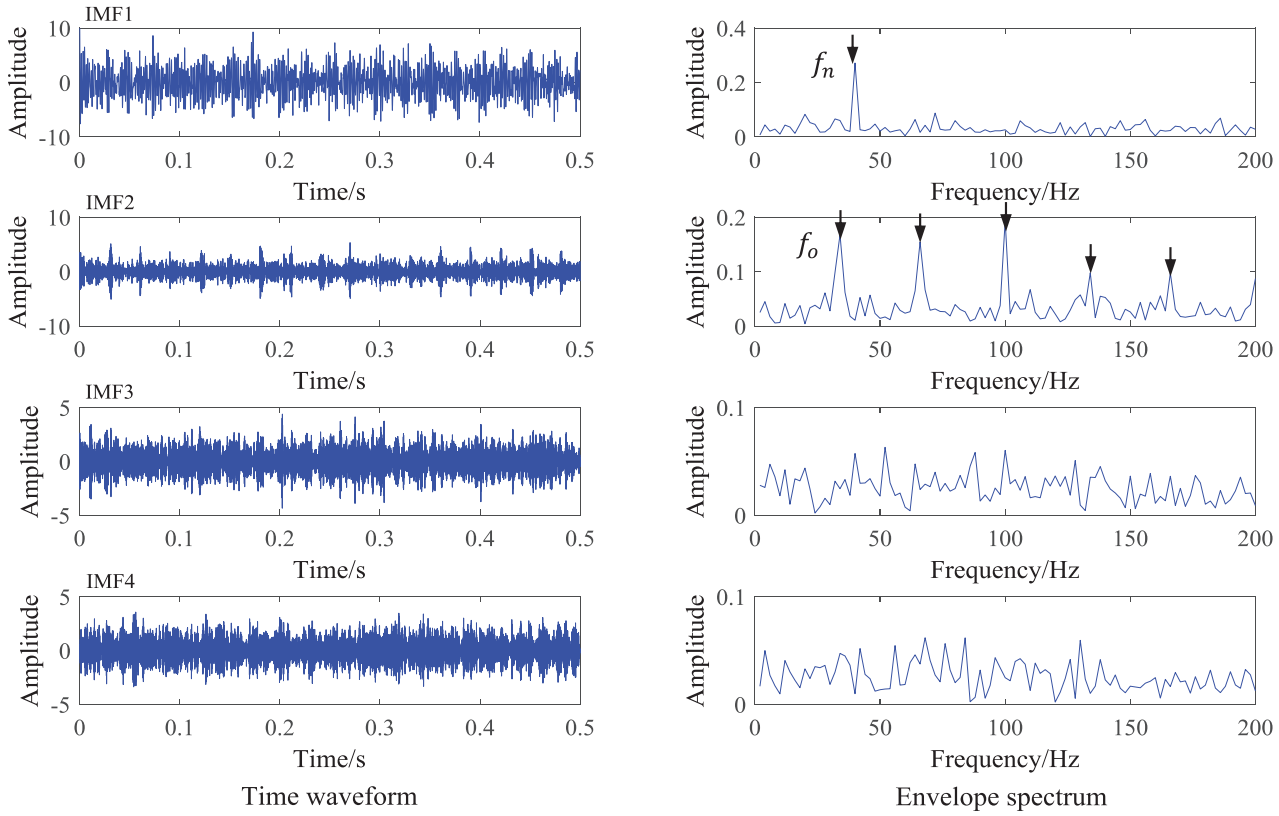

Figure 14. The decomposition results of the gear and bearing compound fault using VMD.

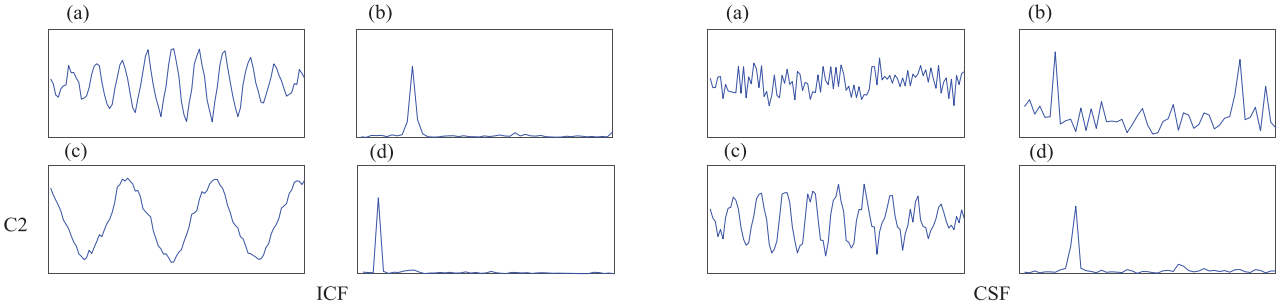

Figure 15. The filters of the gear and bearing compound fault trained by ICF and CSF and the corresponding spectrum. (a) The time waveform of the trained filter of the bearing fault component; (b) the envelope spectrum of the trained filter of the bearing fault component; (c) The time waveform of the trained filter of the first component; (d) the envelope spectrum of the trained filter of the second component.

CSF can only extract the transient component, as shown in figures 13(a) and (b). Figure 15 shows the final filters. It can be seen that the first principle components trained by CSF do not show the gear meshing frequency.

In summary, the simulation analysis results show that the proposed ICF can separate the different fault components and is applicable to all kinds of fault compound mode in strong noise environments.

5. Experimental analysis

The previous sections investigated the decomposition performance of the proposed ICF for various compound fault modes in strong noise environments. In this section, experimental data is employed to further demonstrate the property of ICF. The compound faults of the bearing outer ring fault and gear wear fault were simulated on the experimental platform, as shown in figure 16. In this study, a planet gear and a rolling bearing are selected to simulate the gear fault and the bearing fault. The planetary gear set consists of a sun gear, a ring gear and three planet gears, all remaining in a constant mesh. The number of teeth in the sun gear is 38. The number of teeth of the driven gears is both 18. The tooth surface of the planet gear is ground to simulate the wear failure of the gear. A groove with a width of 0.15 and a depth of about 0.2 is cut in the outer ring of the bearing to simulate the outer ring fault. The acceleration sensor is fixed on the bearing seat at the driving end of the gear box. The driving motor works at 1000 rpm in the testing process. The vibration signals are collected with a sampling frequency of 25.6 kHz, and each vibration sample contains 6400 sample points, as shown in figure 16(a). The filter length L is 100, the number of filters N_f is 20. The separation results of the compound faults are

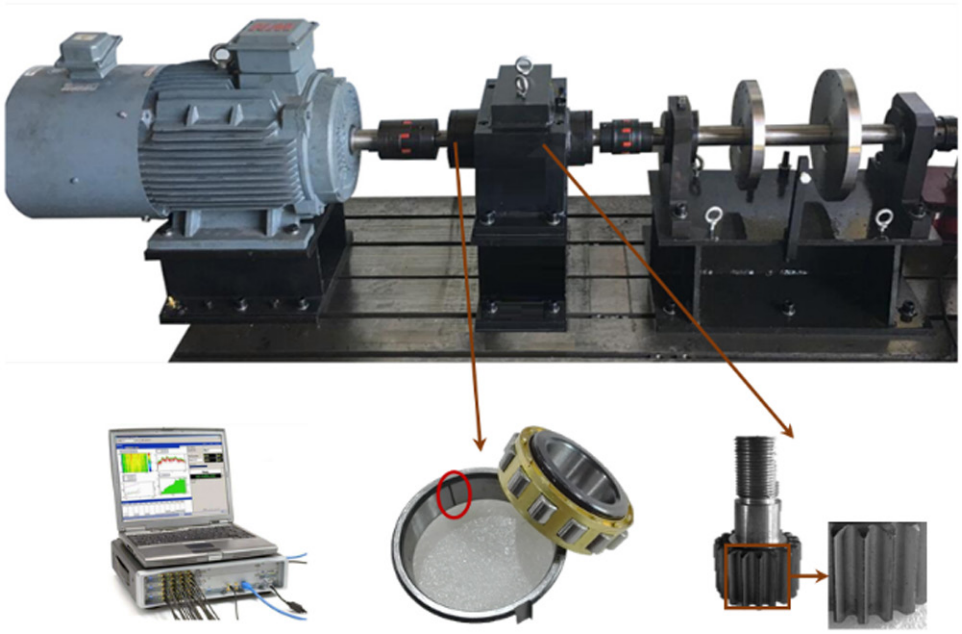

Figure 16. Motor-driven gear box test bench.

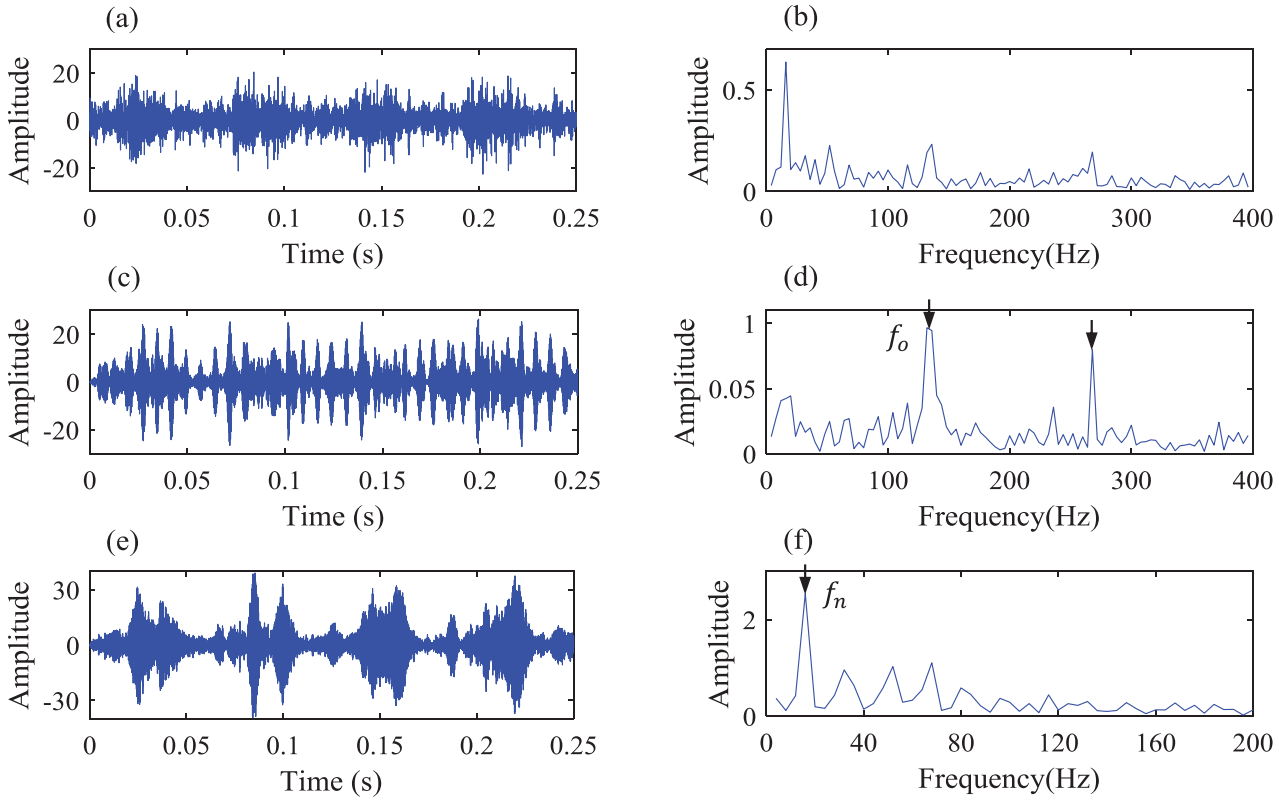

Figure 17. The diagnosis results of the experimental compound fault using ICF. (a) A simulated compound fault vibration time series with SNR $= -10$ dB; (b) the envelope spectrum of the simulated signal; (c) the time waveform of the filtered data of the bearing fault component; (d) the envelope spectrum of the filtered data of the bearing fault component; (e) the time waveform of the filtered data of the gear fault component; (f) the envelope spectrum of the filtered data of the gear fault component.

shown in figures 17 and 18. The ICF can successfully sort out the bearing and gear components in a compound fault. The peak values are obvious at the characteristic frequency of the outer ring and its harmonics, as shown in figure 17(d), which indicates that the bearing has an outer ring fault. In figure 17(f), there is an obvious peak at the rotating frequency, which corresponds to the crack fault of the gear. Compared with CSF, the different fault components are reconstructed better in the time domain.

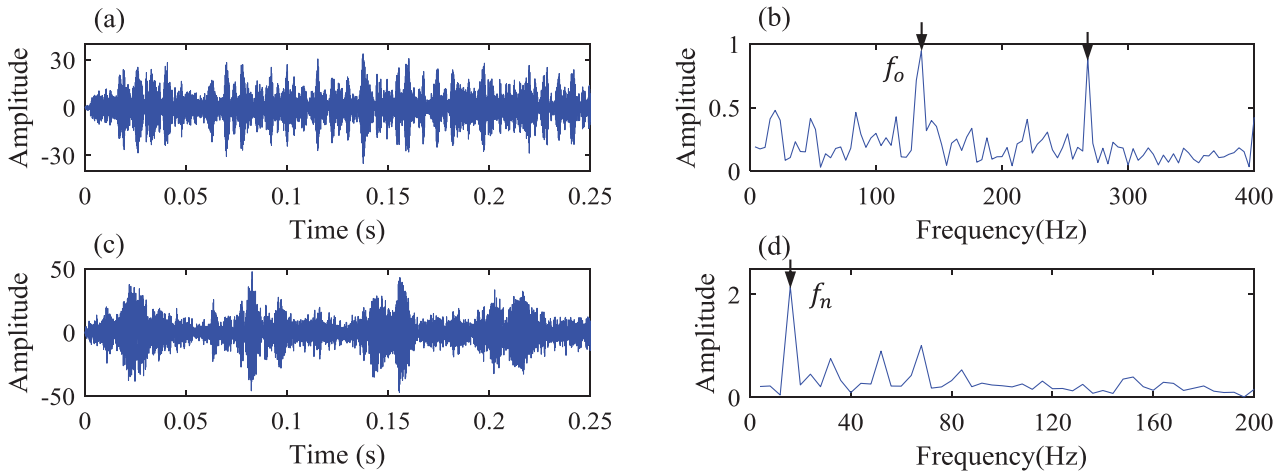

Figure 18. The diagnosis results of the experimental compound fault using CSF. (a) The time waveform of the filtered data of the bearing fault component; (b) the envelope spectrum of the filtered data of the bearing fault component; (c) the time waveform of the filtered data of the gear fault component; (d) the envelope spectrum of the filtered data of the gear fault component.

6. Conclusion

This study proposes a novel compound fault diagnosis method based on intrinsic component filtering applied to the compound fault diagnosis of gearboxes. The proposed method can be divided into three main steps: firstly, a Hankel matrix is constructed as an input by the collected vibration data. Secondly, multiple filters are trained by the intrinsic component filtering in an unsupervised way without any time-consuming preprocessing or a prior basis. Finally, the dominant filter is selected by PCA and Hilbert demodulation analysis is conducted on the filtered data.

The performance of the proposed method is validated by the simulation data and the experiment signals from a planetary gearbox with compound faults. Through the verification results we can obtain the conclusions as follows: the proposed method is a promising tool that can handle different compound fault modes in a strong noise environment. The proposed method shows stronger noise adaptability and robustness, especially for the harmonic component.

It would be very interesting to develop ICF for new applications such as intelligent compound fault diagnosis. The authors will continue to research this topic in the future.

Acknowledgments

The research was supported by the National Natural Science Foundation of China (Grant Nos. 51675262 and 51975276), the National Key Research and Development Program of China (Grant No. 2018YFB2003300), the Advance Research Field Fund Project of China (Grant No. 6140210020102), the Major National Science and Technology Projects (2017-IV-0008-0045) and the Advance Research Field Fund Project of China (Grant No. 61400040304).

ORCID iDs

Zongzhen Zhang https://orcid.org/0000-0002-2022-2116
Yu Xin https://orcid.org/0000-0003-4358-8396

References

[1] Jiang X, Li S and Wang Y 2016 Study on nature of crossover phenomena with application to gearbox fault diagnosis *Mech. Syst. Signal Process.* **83** 272–95
[2] Wang J, Li S, Xin Y and An Z 2019 Gear fault intelligent diagnosis based on frequency-domain feature extraction *J. Vib. Eng. Technol.* **7** 159–66
[3] Ou L and Yu D 2016 Compound fault diagnosis of gearboxes based on GFT component extraction *Meas. Sci. Technol.* **27** 115007
[4] Chen J, Zi Y, He Z and Yuan J 2013 Compound faults detection of rotating machinery using improved adaptive redundant lifting multiwavelet *Mech. Syst. Signal Process.* **38** 36–54
[5] Zhang X and Zhou J 2013 Multi-fault diagnosis for rolling element bearings based on ensemble empirical mode decomposition and optimized support vector machines *Mech. Syst. Signal Process.* **41** 127–40
[6] Miao Y, Zhao M, Makis V and Lin J 2019 Optimal swarm decomposition with whale optimization algorithm for weak feature extraction from multicomponent *Mech. Syst. Signal Process.* **122** 673–91
[7] Wang W J and McFadden P D 1996 Application of wavelets to gearbox vibration signals for fault detection *J. Sound Vib.* **192** 927–39
[8] Fadden P D and Toozhy M 2000 Application of synchronous averaging to vibration monitoring of rolling element bearings *Mech. Syst. Signal Process.* **14** 891–906
[9] Lei Y, Lin J and He Z 2013 A review on empirical mode decomposition in fault diagnosis of rotating machinery *Mech. Syst. Signal Process.* **35** 108–26
[10] Li J and Hao H 2015 Damage detection of shear connectors under moving loads with relative

displacement measurements *Mech. Syst. Signal Process.* **60–1** 124–50
[11] Jiang H, Li C and Li H 2013 An improved EEMD with multiwavelet packet for rotating machinery multi-fault diagnosis *Mech. Syst. Signal Process.* **36** 225–39
[12] Jiang X, Li S and Wang Q 2016 A novel method for adaptive multiresonance bands detection based on VMD and using MTEO to enhance rolling element bearing fault diagnosis *Shock Vib.* **1** 1–9
[13] Miao Y, Zhao M and Lin J 2019 Identification of mechanical compound-fault based on the improved parameter-adaptive variational mode decomposition *ISA Trans.* **84** 82–95
[14] McDonald G, Zhao Q and Zuo M 2012 Maximum correlated Kurtosis deconvolution and application on gear tooth chip fault detection *Mech. Syst. Signal Process.* **33** 237–55
[15] Miao Y, Zhao M, Lin J and Lei Y 2017 Application of an improved maximum correlated kurtosis deconvolution method for fault diagnosis of rolling element bearings *Mech. Syst. Signal Process.* **92** 173–95
[16] Hong L, Liu X and Zuo H 2018 Compound fault diagnosis of rotating machinery based on adaptive maximum correlated kurtosis deconvolution and customized multiwavelet transform *Meas. Sci. Technol.* **29** 115007
[17] Starck J, Elad M and Donodo D 2004 Redundant multiscale transforms and their application for morphological component separation *Adv. Imaging Electron Phys.* **132** 287–384
[18] Antoni J and Randall R B 2006 The spectral kurtosis: application to the vibratory surveillance and diagnostics of rotating machines *Mech. Syst. Signal Process.* **20** 308–31
[19] Antoni J 2007 Fast computation of the Kurtogram for the detection of transient faults *Mech. Syst. Signal Process.* **21** 108–24
[20] Xu Y G, Zhang K, Ma C Y, Cui L and Tian W K 2019 Adaptive Kurtogram and its applications in rolling bearing fault diagnosis *Mech. Syst. Signal Process.* **130** 87–107
[21] Chen B, Zhang Z, Zi Y, He Z and Sun C 2013 Detecting of transient vibration signatures using an improved fast spatial—spectral ensemble kurtosis Kurtogram and its applications to mechanical signature analysis of short duration data from rotating machinery *Mech. Syst. Signal Process.* **40** 1–37
[22] Wang D, Peter W T and Tsui K L 2013 An enhanced Kurtogram method for fault diagnosis of rolling element bearings *Mech. Syst. Signal Process.* **35** 176–99
[23] Lei Y, Lin J, He Z and Zi Y 2011 Application of an improved Kurtogram method for fault diagnosis of rolling element bearings *Mech. Syst. Signal Process.* **25** 1738–49
[24] Miao Y, Zhao M and Lin J 2017 Improvement of kurtosis-guided-grams via Gini index for bearing fault feature identification *Meas. Sci. Technol.* **28** 125001
[25] Bobin J, Starck J, Fadili J, Moudden Y and Donoho D 2007 Morphological component analysis: an adaptive thresholding strategy *IEEE Trans. Image Process.* **16** 2675–81
[26] Yu D, Wang M and Cheng X 2016 A method for the compound fault diagnosis of gearboxes based on morphological component analysis *Measurement* **91** 519–31
[27] Tang G, Wang X and He Y 2016 Diagnosis of compound faults of rolling bearings through adaptive maximum correlated kurtosis deconvolution *J. Mech. Sci. Technol.* **30** 43–54
[28] Ngiam J, Chen Z, Bhaskar S, Koh P and Ng A 2011 Sparse filtering, *Proc. Neural Inf. Process. Syst.* 1125–33
[29] Lei Y, Jia F, Lin J, Xing S and Ding S 2015 An intelligent fault diagnosis method using unsupervised feature learning towards mechanical big data *IEEE Trans. Ind. Electron.* **63** 3137–47
[30] Zhang Z, Li S, Wang J, Xin Y and An Z 2019 General normalized sparse filtering: a novel unsupervised learning method for rotating machinery fault diagnosis *Mech. Syst. Signal Process.* **124** 596–612
[31] Jia X, Zhao M, Di Y, Jin C and Lee J 2017 Investigation on the kurtosis filter and the derivation of convolutional sparse filter for impulsive signature enhancement *J. Sound Vib.* **386** 433–48
[32] Jia X, Zhao M, Di Y, Li P and Lee J 2018 Sparse filtering with the generalized $l_p l_q$ norm and its applications to the condition monitoring of rotating machinery *Mech. Syst. Signal Process.* **102** 198–213